



Field spectroscopy for the detection of underground military structures

George Melillos, Athos Agapiou, Kyriacos Themistocleous, Silas Michaelides, George Papadavid & Diofantos G. Hadjimitsis

To cite this article: George Melillos, Athos Agapiou, Kyriacos Themistocleous, Silas Michaelides, George Papadavid & Diofantos G. Hadjimitsis (2019) Field spectroscopy for the detection of underground military structures, European Journal of Remote Sensing, 52:1, 385-399, DOI: [10.1080/22797254.2019.1625075](https://doi.org/10.1080/22797254.2019.1625075)

To link to this article: <https://doi.org/10.1080/22797254.2019.1625075>



© 2019 The Author(s). Published by Informa UK Limited, trading as Taylor & Francis Group.



Published online: 03 Jun 2019.



Submit your article to this journal [↗](#)



Article views: 85



View Crossmark data [↗](#)

Field spectroscopy for the detection of underground military structures

George Melillos, Athos Agapiou, Kyriacos Themistocleous, Silas Michaelides, George Papadavid and Diofantos G. Hadjimitsis

Department of Civil Engineering and Geomatics, Faculty of Engineering and Technology, Cyprus University of Technology, Limassol, Cyprus

ABSTRACT

Remote sensing is considered as an increasingly important technology for military intelligence. New satellite missions, such as Sentinel 2A, may provide systematic datasets for monitoring vast areas of interest. However, there is a great need to understand the information retrieved from such sensors. This paper contemplates the results obtained from a one-year field spectroradiometer campaign, aiming at the detection of underground military structures in Cyprus, covered with crops. The measurements were taken at the following test areas: (a) vegetation area covered with vegetation (barley), in the presence of an underground military structure, and (b) vegetation area covered with vegetation (barley), in the absence of an underground military structure. The ground hyperspectral signatures were resampled to the Sentinel-2A sensor using the appropriate Relative Spectral Response Filters (RSRF). Ten vegetation indices were utilized for the identification of the detection of underground military structures. Results have shown that differences exist between these ten vegetation indices, thus some of them are sufficient to distinguish the two areas. The phenological analysis of these measurements have shown the period of head emergence stage is suitable for monitoring crop marks. Sentinel-2A results were also validated with field spectroradiometer results which were acquired during a simultaneous in-situ campaign.

ARTICLE HISTORY

Received 19 April 2018
Revised 21 April 2019
Accepted 25 May 2019

KEYWORDS



Remote sensing;
spectroscopy; military
underground structures;
vegetation indices

Introduction

For decades, research on the detection of buried targets has led to the development of a variety of techniques for identifying buried structures (Piper, Lim, Thorsos, & Williams, 2009; Zhang, Liao, & Carin, 2004). These techniques use a variety of geophysical instruments (Apparao, Gangadhara Rao, Sivarama Sastry, & Subrahmanya Sarma, 1992; Kelly, 2001; Mahrer, 1995; Stolarczyk, 1993) that measure gravitational, electric and magnetic fields, as well as sound waves to detect underground remains (Milton & Rollin, 2006). The premise of these instruments is that structures can be identified by the altered features of the Earth, such as differences in rock density and porosity, soil moisture and magnetic fields, thereby indicating the presence or absence of underground structures.

A lot of attention is being paid to the development of new methods and instrumentation for the detection of buried targets. Field spectroscopy for the detection of military underground structures is a major concern for military and national security agencies (Melillos et al., 2016a). This is evident the large budget (Department of the Army, 2006) allocated for the detection and monitoring of military underground

structures. Currently, national security agencies use Human Intelligence (HUMINT) which refers to human sources as a tool and a variety of collection methods. HUMINT is defined as the collection of information by a trained HUMINT collector (military occupational specialties) (Department of the Army, 2006), from people and their associated documents and media sources for the identification of elements, intentions, composition, strength, dispositions, tactics, equipment, personnel and capabilities. However, technology such as imagery intelligence (IMINT) can also be used for gathering information. Imagery intelligence (IMINT) is defined by the USA Department of Defense (DOD) as intelligence derived from the exploitation of collection by visual photography, infrared sensors, lasers, electro-optics and radar sensors such as synthetic aperture radar, whereby images of objects are reproduced optically or electronically on film, electronic display devices, or other media (Crothers, Lanphear, Garino, Konyha, & Byrne, 1967; IOSS, 2017). Remote sensing techniques are quick, easily manageable and involve a wide variety of techniques where valuable information can be accessed remotely (Canada Centre for Remote Sensing, 2016; Garaba & Zielinski, 2015). Ground spectroradiometric measurements can provide the spectral response of the vegetation in detail (Sepp, 2000).

CONTACT George Melillos  gmelillos@gmail.com  Department of Civil Engineering and Geomatics, Faculty of Engineering and Technology, Cyprus University of Technology, Limassol, Cyprus

This article has been republished with minor changes. These changes do not impact the academic content of the article.

© 2019 The Author(s). Published by Informa UK Limited, trading as Taylor & Francis Group.

This is an Open Access article distributed under the terms of the Creative Commons Attribution License (<http://creativecommons.org/licenses/by/4.0/>), which permits unrestricted use, distribution, and reproduction in any medium, provided the original work is properly cited.

Buried underground structures are difficult to detect, especially when they are fully covered by soil (IOCCG, 2008). It is possible to detect these military underground structures by means of satellite images and aerial photographs. The concern about underground facilities (or “hard and buried” targets) is evident from the establishment of several purpose-dedicated components within various intelligence and defense agencies (Papadavid, Hadjimitsis, Michaelides, & Nisantzi, 2011). A reasonable solution may be found by combining traditional geological and geochemical techniques with remote sensing. The initial evaluation and interpretation of remote sensing data provides information about the location (Richelson, 2013). Using a concomitant interpretation of satellite and ground data, maps can be compiled which can reveal areas where “buried” underground structures are located. This is achieved by documenting and assessing soil anomalies and by interpreting vegetation anomalies which may serve as indicators; this can be realized through a combination of terrestrial and satellite data. Therefore, surveys can be carried out at different times to document the evolution of the area on a systematic basis. Moreover, sensors sensitive to different ranges of the electromagnetic spectrum allow the recognition of different types of ground cover. A range of digital processing procedures can be used to enhance the images (Richelson, 2013).

Underground structures such as military structures, military bunkers and bases, tunnel networks and archaeological remains can affect their surrounding landscapes in different ways, including changes in thermal inertia (Gunn et al., 2008), localized soil moisture content and drainage rates (KMC, 2008), soil composition and vegetation vigor (Milton & Rollin, 2006). Vegetation vigor is often observed on the ground as a crop mark, a spot which can be used to denote the presence of underground structures (Lasaponara & Masini, 2006). Crop marks can be formed both as negative marks above wall foundations and as positive marks above the damper and more nutritious soil of buried pits and ditches (Lasaponara & Masini, 2006).

During the last decade, enhancements in sensor characteristics, as well as technological achievements in space technology, offer new opportunities for future applications (Giardino, 2011); in this respect, examples include the hyperspectral satellite sensor with 30 m resolution which can be traced back in 2000 when EO1 Hyperion was launched, and the airborne sensor AVIRIS that was developed by NASA-JPL in 1983.

Literature review

In this context, it should be noted that, in some cases, researchers seek to find not the target itself but rather

to identify symptoms related to the topography (relief), crop characteristics (crop marks), soil characteristics (soil marks) or even changes in snow cover (snow marks). For instance, archaeological structures buried beneath the soil (i.e. still un-excavated sites) can be detected through remote sensing images as stressed vegetation (crop marks) which can be used as a proxy for the buried archaeological relics. Crop marks may be formed in areas where vegetation grows over near-surface archaeological remains. These features modify the moisture retention compared to the rest of the crop coverage of an area. Depending on the type of the feature, crop vigor may be enhanced or reduced by buried archaeological features (Winton & Horne, 2010).

If vegetation grows above buried ditches or moat, then the crop growth is likely to be enhanced. This is due to the topsoil, which holds more moisture than in the surrounding context (especially during periods of water stress). This contrasting phenomenon can be recorded from a suitable airborne or space borne platform and is referred to as a positive crop mark (Lasaponara & Masini, 2006; Agapiou et al., 2012a). However, in cases where there is not enough moisture in the retentive soil and there is lack of available water for evapotranspiration (e.g. vegetation grown above building remains or compacted ground), the marks developed are characterized as negative crop marks which are less common than positive crop marks (Lasaponara & Masini, 2007; Riley, 1979). In comparing the two different kinds of marks, the positive crop marks are normally taller with darker green and healthy foliage than the negative crop marks, while negative crop marks tend to be paler green with lighter colored appearance when monitored from the air (Johnson, 2006). However, the field spectroscopy for the detection of such crop marks still comprises a difficult task since these marks may not be visible in the images if observed over different time periods or at different spatial/spectral resolutions. Previous research such as detecting and imaging of underground installments (e.g. tunnels, bunkers) in a hostile environment poses unique challenges on deployment and remote sensing methods (ARO, 2018). Despite the technological improvements, both in terms of the sensitivity of the sensors (spectral characteristics) and in terms of spatial resolution of satellite datasets, new methods and algorithms are essential to improve Earth observation remote sensing technologies for supporting military research (Themistocleous, Agapiou, Cuca, & Hadjimitsis, 2015). Spectral Remote Sensing is found to be widely used in several purposes for the detection underground structures such as agriculture remains (Agapiou et al., 2012a)

In addition, Spectral Remote Sensing for the detection of underground military structures, is considered

to be very precise in detecting sub-surface remains. Different geophysical processing techniques and equipment, such as ground penetrating radar (GPR), magnetometer and resistivity are usually integrated to maximize the success rate of uncovering underground remains (Domínguez Galindo, Bandy, Mortera Gutiérrez, & Ortega Ramírez, 2013; Novo, Solla, Fenollós, & Lorenzo, 2014; Sarris et al., 2004, 2013). Moreover, the use of unmanned aerial vehicles (UAVs, popularly known as drones) for environmental remote sensing purposes has increased in recent years. Although the military has used UAVs in defense applications for decades, the scientific environmental sector increasingly takes advantage of the application of UAVs (D'Oleire-Oltmanns, Marzolf, Peter, & Ries, 2012).

This paper investigates also the potential of applying Sentinel 2A satellite data to field data in order to distinguish between a buried structure (existence of underground structure) area and a vegetated area (no existence of underground structure). The Sentinel 2A satellite sensor is the first optical Earth Observation satellite in the European Copernicus programme and was developed and built under the industrial leadership of Airbus Defense and Space for the European Space Agency (ESA). The span of 13 spectral Bands, from the visible and the near-infrared to the short-wave infrared at different spatial resolutions ranging from 10 to 60 m on the ground, promotes global land monitoring to an unprecedented level. Sentinel-2A satellite is the first civil optical Earth Observation mission of its kind to include three Bands in the “red edge”, which provide key information on the vegetation state (ESA, 2018).

In the literature, it is noted that there is a gap in the monitoring of vegetation over military underground and ground structures throughout the plants' phenological development cycle; this paper aspires to contribute to the filling-in of this gap. This study aims to present the results obtained from ground spectroradiometric campaigns, using a SVC-HR1024 field spectroradiometer, carried out in a specific area in Cyprus. Field spectroradiometric measurements were collected and analyzed to identify a known underground structure using the spectral profile of the vegetated surface over the underground target and the surrounding area for in situ observations. Crop marks can reveal the presence and the absence of military underground structures not visible from the satellite images.

Materials and methods

This study proposes a methodology for detecting underground targets using remote sensing techniques. The basis of this methodology is the combination of the study of the vegetation phenology as

a proxy for buried underground structures of defense significance. Data acquisitions were used to identify any variations between the area over an underlying structure and over a reference area.

For this study, certain assumptions have been adopted. In this study, certain assumptions have been adopted which have a critical impact on the findings. In this project, phenological field observations were conducted at two test sites from 2016 to 2017 in order to determine the dates of completion of different phenological phases. For actual defense purposes, the characteristics of the target and especially the area of interest are often not known, such as for example, the depth below the ground surface at which the military underground structures are located, the horizontal dimensions of the underground structure and the soil type. Furthermore, the cultivation of barley in the area is for investigative purposes and part of the experimental work for studying the impact of underlying structures on vegetation. Under real scenarios, different types of vegetation (if any) will be present.

Study area

Due to security and confidentiality issues, the specific area cannot be reported herein. The proposed methodology has been applied in Cyprus over a specific geographical area. The area is situated on a hill which provides clear viewing from airborne and spaceborne platforms, making the area ideal for remote sensing applications (Figure 1, left). Also, it is located within a fenced, abandoned military area. The soil type of the area is leptosol which contains small amounts of gravel and with a very shallow depth.

Figure 1 (right) shows a military storage bunker similar to the one that is in the focus of this research. The horizontal dimensions of the underground structure are 13 m × 5 m; it is a concrete storage bunker, located approximately 2 m below the ground surface.

Methodology

Spectral data are increasingly incorporated into process-based models of the Earth's surface and the atmosphere. The area of interest was determined first by identifying plots with a high probability of buried targets. Such areas can be determined from various sources, such as on-site irregular activities, personal communication, surveys and crop marks.

The in-situ measurements were resampled to the Sentinel-2A data using the appropriate Relative Spectral Response filters. Several different UAVs were used including a DJI Inspire 2 and DJI Phantom, equipped with cameras, and flown at an altitude of 5, 10, and 20 meters above the ground.



Figure 1. Overview of the study area (left); an example of a military bunker (right).

In-situ measurements were taken at two test areas: (a) vegetation area covered with vegetation (barley), in the presence of an underground military structure [hereafter denoted as Area (a)], and (b) vegetation area covered with vegetation (barley), in the absence of an underground military structure [hereafter denoted as Area (b)].

An SVC-1024 spectroradiometer from the Spectra Vista Corporation (SVC) with a spectral range of 350–2500 nm was used to measure reflectance values. The spectral resolution of the Spectroradiometric 1.0 nm. The measurements were taken between 11:00 am and 13:00 pm (Local Time), under clear and overcast skies for diffuse light to minimize any variation of the incoming solar electromagnetic radiance. In addition, a calibrated spectralon panel (with reflectance $\approx 99.996\%$) measurement was used as a reference, while the measurement over the crops were used as a target (Papadauid et al., 2011).

The spectral reflectance values were used to calculate vegetation indices (VIs) such as the Normalized Difference Vegetation Index (NDVI), Enhanced Vegetation Index (EVI), Simple Ratio (SR), Renormalized Difference Vegetation Index (RDVI),

Red Green Ratio Index (IRG), Ratio Vegetation Index (RVI), Optimized Soil Adjusted Vegetation Index (OSAVI), Difference Vegetation Index (DVI), Global Environment Monitoring Index (GEMI) and Modified Simple Ratio (MSR), as shown in Table 1. The wave Band reflectance was calculated from the Relative Spectral Response (RSR) filter of the Sentinel-2A sensor (with GSD 10 m). The vegetation indices were plotted and statistically cross compared between the two areas of interest namely the “buried military structure” and the “non-military structure”.

In-situ measurements were taken in a grid format just as the dimension of the underground structure (13 m \times 5 m) over the two study areas. Measurements were well spread in each structure, were made randomly and collected in order to have a representative sample that was statistically reliable. The measurements were taken in the middle and around the underground structure. Due to the very close proximity of the two sites (less than 20 m), the analysis was based on the following two criteria: the first is that both study areas have similar soil and the second is that both areas have climatic characteristics (Agapiou and Hadjimitsis, 2011a). The Area (a) is the area over

Table 1. Vegetation indices used in this study, where p_{NIR} , p_{RED} , p_{BLUE} and p_{GREEN} represent the atmospherically or partially atmospherically corrected surface reflectance values of the near-infrared (NIR), red (RED), blue (BLUE) and green (GREEN) wavelengths, respectively (Melillos et al., 2016a).

No.	Vegetation Index	Equation	Reference
1.	NDVI (Normalized Difference Vegetation Index)	$(p_{\text{NIR}} - p_{\text{RED}}) / (p_{\text{NIR}} + p_{\text{RED}})$	(Rouse, Haas, Schell, Deering, & Harlan, 1974)
2.	EVI (Enhanced Vegetation Index)	$2.5 (p_{\text{NIR}} - p_{\text{RED}}) / (p_{\text{NIR}} + 6p_{\text{RED}} - 7.5 p_{\text{BLUE}} + 1)$	(Huete, Liu, Batchily, & van Leeuwen, 1997)
3.	SR (Simple Ratio)	$p_{\text{NIR}} / p_{\text{RED}}$	(Jordan, 1969)
4.	RDVI (Renormalized Difference Vegetation Index)	$(p_{\text{NIR}} - p_{\text{RED}}) / (p_{\text{NIR}} + p_{\text{RED}})^{0.5}$	(Roujean & Breon, 1995)
5.	IRG (Red Green Ratio Index)	$p_{\text{RED}} - p_{\text{GREEN}}$	(Gamon & Surfus, 1999)
6.	RVI (Ratio Vegetation Index)	$p_{\text{RED}} / p_{\text{NIR}}$	(Pearson & Miller, 1972)
7.	OSAVI (Optimized Soil Adjusted Vegetation Index)	$(p_{\text{NIR}} - p_{\text{RED}}) / (p_{\text{NIR}} + p_{\text{RED}} + 0.16)$	(Rondeaux, Steven, & Baret, 1996)
8.	DVI (Difference Vegetation Index)	$p_{\text{NIR}} - p_{\text{RED}}$	(Tucker, 1979)
9.	MSR (Modified Simple Ratio)	$p_{\text{RED}} / (p_{\text{NIR}} / p_{\text{RED}} + 1)^{0.5}$	(Chen, 1996)
10.	GEMI (Global Environment Monitoring Index)	$n(1 - 0.25 n)(p_{\text{RED}} - 0.125) / (1 - p_{\text{RED}})$ $n = [2(p_{\text{NIR}}^2 - p_{\text{RED}}^2) + 1.5 p_{\text{NIR}} + 0.5 p_{\text{RED}}] / (p_{\text{NIR}} + p_{\text{RED}} + 0.5)$	(Pinty & Verstraete, 1992)

the underground structure itself and the area around it. The Area (b) is the reference area; absence of an underground military structure. The measurements were also made when the underground structure was covered with the existing natural soil which was subsequently cultivated and covered with vegetation (barley), in order to study possible differences of the spectral signature of vegetation, as a result of the existence of underground structures. A SVC-HR 1024 field spectroradiometer which has a spectral range of 350–2500 nm was used to acquire in-situ spectral data, while in-Band reflectances were determined from medium and high-resolution satellite sensors, such as Sentinel 2A. A calibrated spectralon panel (with reflectance $\approx 100\%$) measurement was used as a reference, while the measurement over the crops were used as a target. The height of measurement was about 1 meter above the ground. During the campaign, 1740 measurements were taken using SVC-1024; an average reference spectral signal is given for the six campaigns in Table 2.

During the in-situ measurements, meteorological data, site characteristics and measurement methods were recorded (Riley, 1979), including information such as the geographical location of the site (latitude and longitude; this data is not allowed to be presented in this article). In addition, the following were also recorded: time of measurement, cloud cover, details on reference panel, viewing geometry and instrument support (mast, tripod, hand-held), height of measurements above target and the delay between target and reference panel measurements.

The case study was monitored throughout the phenological cycle of the crops (Figure 2). The phenological cycle is defined as a series of stages or phases in the seasonal cycle of a plant that can be defined by start and end points. Observable changes in each crop cycle can be identified in Figure 2 that features how barley grows during its life-cycle. In Figure 2, each photo represents a phenological stage of barley, starting from the stage of cultivation and ending with the stage of “drying foliage”. In addition, spectral signatures for each phenological stage, illustrated by graphs and close-up photos, as shown in Figure 2.

Relative differences of VIs for the detection of crop marks

For an evaluation of the performance of all VIs during the phenological cycle of the barley crop, the

relative difference in contrast of the measurements between the “buried structure area” and “vegetated area” was examined. The maximum values for the whole phenological cycle were calculated for the “buried structure area” and “vegetated area”, so that all vegetation indices were normalized. This is essential, since the absolute values of several VIs are not normalized, while at the same time, several variations may be recorded during the same or different phenological observations (Agapiou et al., 2012b). The following relationship was used to calculate the relative difference in contrast, between the “buried structure area” and “vegetated area”.

$$VI \text{ r.d.c} = [(VI \text{ b.s.a} - VI \text{ v.a.}) / (VI \text{ v.a.})] \times 100 \quad (1)$$

where:

VI r.d.c: the VI value for relative difference in contrast;

VI b.s.a: the VI value over the “buried structure area”;

VI v.a.: the VI value over the “vegetated area”.

Results

Waveband reflectance scatterplots

Initially, the Sentinel-2A VINIR reflectance values for Area (a) (buried structure) and Area (b) (vegetated area) were plotted as demonstrated in Figure 3(a–d). This correlation takes each pair of satellite Bands and computes the correlation coefficient between the Bands reflectance to identify the conceptual Band. This Figure shows the results for the green Band (0.560 nm) versus red Band (0.665 nm) (Figure 3(a)), blue Band (0.490 nm) versus NIR Band (0.842 nm) (Figure 3(b)), red Band versus NIR Band (Figure 3(c)) and green Band versus NIR Band (Figure 3(d)). The scatter plots visualize the difficulty to distinguish the two areas (Area (a) and Area (b) especially in the first phenological stages of the barley crops. In the visible part of the spectrum (Figure 3(a)) the separability between the two samples is quite low while this is increased only with the use of the NIR part of the spectrum (see Figure 3(b–d)). This was expected also from the spectral profile of the crops which tend to give very high reflectance values at the NIR part of the spectrum compared to the visible part.

Table 2. Number of measurements in whole phenological stage.

No.	Date	Phenological stage	Number of Measurements	Time of measurements	Humidity	Temp	Weather
(a)	30–10–2016	Cultivation Stage	120	12:10	31%	22°C	Passing clouds.
(b)	11–12–2016	Tilling Stage	120	12:05	60%	18°C	Passing clouds.
(c)	23–01–2017	Flag Leaf Emerging Stage	120	12:36	77%	16°C	Passing clouds.
(e)	25–02–2017	Boot Stage	460	12:48	57%	17°C	Scattered clouds.
(f)	05–03–2017	Head Emerging stage	460	12:10	41%	18°C	Sunny
(g)	16–03–2017	Flowering stage	460	12:15	55%	19°C	Partly sunny







No.	Date	Phenological stage	Temperature		Photo
			Humidity		
(a)	30-10-2016	Cultivation Stage	22 °C	31%	
(b)	11-12-2016	Tilling Stage	18 °C	60%	
(c)	23-01-2017	Flag Leaf Emerging Stage	16 °C	77%	
(d)	25-02-2017	Boot Stage	17 °C	57%	
(e)	05-03-2017	Head Emerging stage	18 °C	41%	
(f)	16-03-2017	Flowering stage	19 °C	55%	

Figure 2. Phenological stages of barley crops with spectral signatures and photos. (a) 20–11–2016, cultivation stage;(b) 11–12–2016, tilling stage; (c) 21–12–2016, advanced tilling stage; (d) 21–12–2016, advanced tilling stage; (e) 18–02–2017, flag leaf fully emerging stage; (f) 25–02–2017, boot stage; (g) 05–03–2017, head emerging stage; (h) 27–03–2017, flowering stage.

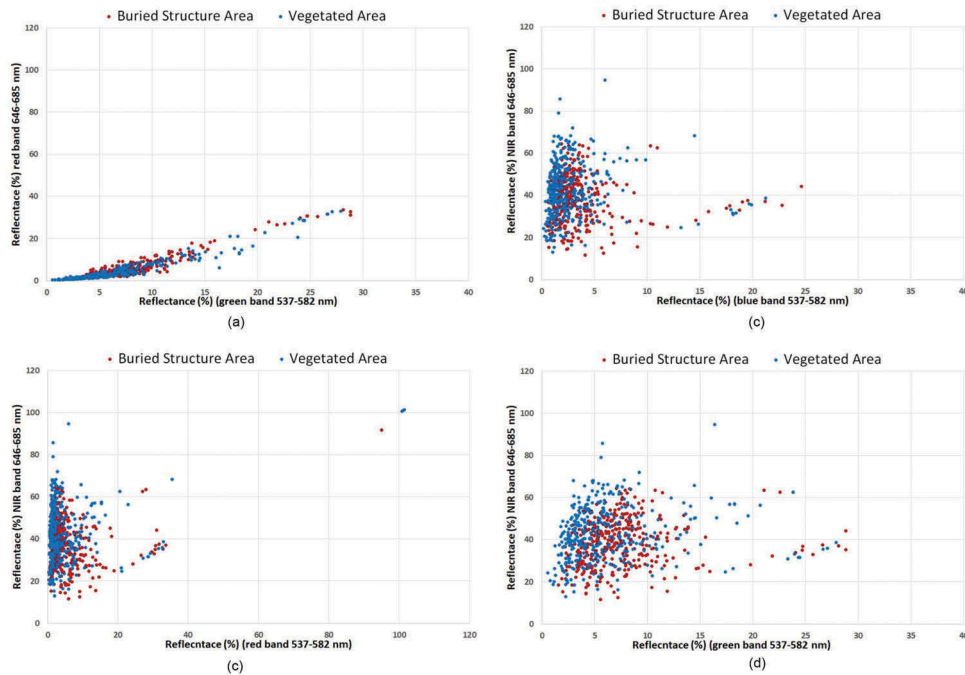


Figure 3. Spectral scatter plots for the area (a) (buried structure – red dots) and area (b) (vegetated area -blue dots) for: (a) green band versus red band; (b) blue band versus NIR band; (c) red band versus NIR band; and (d) green band versus NIR band.

Vegetation indices (VIs)

Figure 4(a–j) show the results of the vegetation indices shown in Table 1 during phenological stage. The vegetation indices were applied to the barley crops over the buried structure (BA) (red dots) and vegetated area (VA) (blue dots). We evaluated the response of Vegetation index values to barley growth with a comparison in the above-mentioned areas. The results showed that VIs obtain distinct variation corresponding to barley development and they could be used as cultivar-independent phenological indicators. It can be observed, that there is a high correlation between the results of VIs. Indeed, VIs could be used as a single threshold using Field spectroscopy for the detection of buried structures. The use of more than one VIs for the detection of crop marks is suggested to enhance the final results. Furthermore, it is clear from these diagrams that VIs values vary from one phenological stage to another. Although the same dataset was used for all these vegetation indices, each of the VIs demonstrates a different response at the different phenological stages. It may be seen clearly in the flowering stage that there is distinct differentiation between BA and VA. There is an upward trend of VA (blue dots) compared to BA (red dots) which exhibits a downward trend. Evidently, this happens in all VIs except for OSAVI (Figure 4(g)), IRG (Figure 4(e)), RVI (Figure 4(f)) and MSR. As growth stages progress, the ground spectral signatures of BA (red dots) for DVI (Figure 4(h)), IRG (Explicitly, using GEMI index, BA (red dots) tends to exhibit a difference with respect to VA (blue dots). More specifically, in target area BA (red

dots), the reflectance response is higher than area VA (blue dots) throughout the phenological stages, which indicates that the resulting differences reinforce the existence/non-existence of underground structures.

Relative differences of VIs for the detection of crop marks

Based on the formula to calculate the relative difference in contrast, between the “buried structure area” and “vegetated area”, the following results displayed in Figure 5 were extracted for NDVI, EVI, SR, RDVI, IRG, RVI, OSAVI, DVI, GEMI and MSR. Examining the results from the VIs, it was found that the relative reference in contrast is maximized for all indices when the crop begins to grow (from the end of December until the end of March). There is a high performance for all indices during the head emerging stage. At this stage, MSR, RVI, IRG, SR, EVI and GEMI seem to be the most suitable indices. The DVI index is also another VI worthy to consider. One other important information on this chart is that the MSR and RVI vegetation indices are higher than other VIs during the head emerging stage. Also, SR and GEMI are consistently high during all phenological stages. The most interesting observation regarding these values is the fact that they were observed during the same phenological stage.

A *t*-test was also performed to evaluate and to compare the difference between the two areas (average values) in the different phenological stages using the following equation:

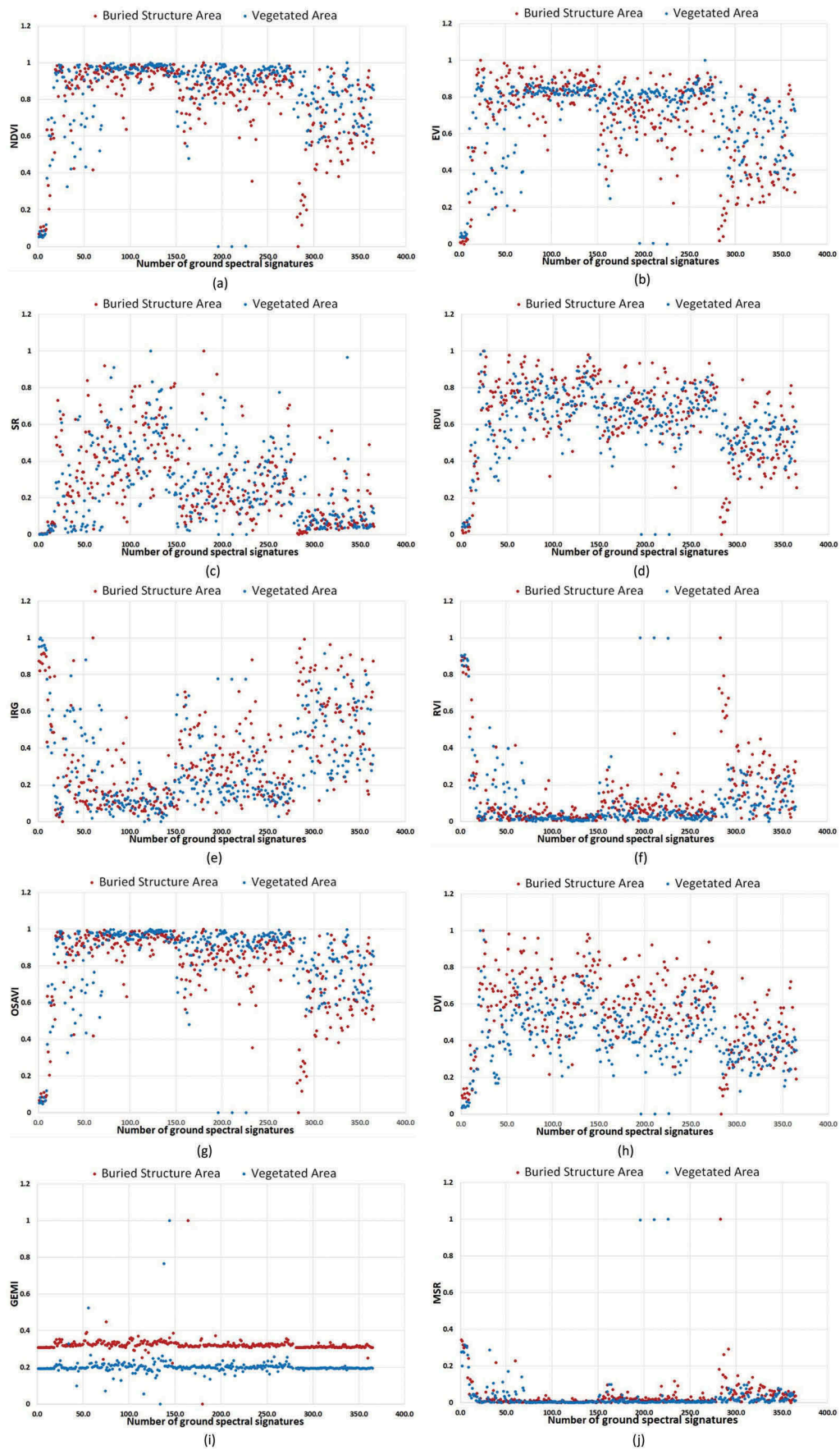


Figure 4. Vegetation values for the area (a) for (buried structure – red dots) and area (b) for (vegetated area -blue dots) during phenological cycle for: (a) NDVI, (b) EVI, (c) SR, (d) RDVI, (e) IRG, (f) RVI, (g) OSAVI, (h) DVI, (i) GEMI, and (j) MSR.

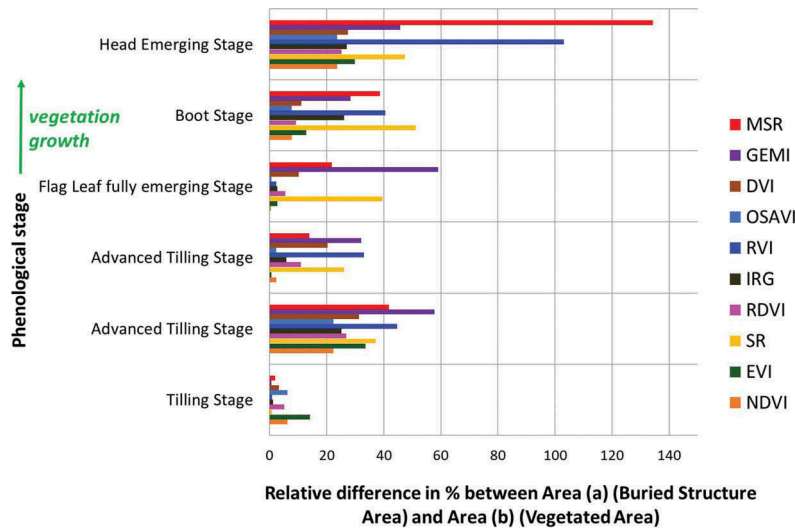


Figure 5. Relative difference in % between area (a) (buried structure area) and area (b) (vegetated area) for NDVI, EVI, SR, RDVI, IRG, RVI, OSAVI, DVI, GEMI and MSR.

$$t = \frac{(X_1 - X_2)}{\sqrt{\frac{(S_1)^2}{n_1} + \frac{(S_2)^2}{n_2}}}$$

Where,

- X_1 = Mean of first set of values
- X_2 = Mean of second set of values
- S_1 = Standard deviation of first set of values
- S_2 = Standard deviation of second set of values
- n_1 = Total number of values in first set
- n_2 = Total number of values in second set.

As shown in Figure 6, the critical t (t -critical) was found at 2.1. Also, the number of degrees of freedom was found at 83 value and alpha level at 0.05 value. Although in the first four phenological stages the t -static is mainly lower than the t -critical, except for IRG, SR, RDVI and DVI, and hence the difference between the two samples (BA and VA) is not

statistically significant, the last two phenological stages (i.e. boot stage and head emerging stage) are considered as the most suitable for observing these vegetation anomalies. During this period, all the vegetation indices mentioned in Table 1 as well the Band reflectances provide statistically significant differences among the two samples. It should be mentioned that this optimum period was also reported in Agapiou, Hadjimitsis, Sarris, Georgopoulos, and Alexakis (2013). Similarly, examining the results from the t -test (Figure 6), it was found that during the phenological stage, the t -statistic is increase during the head emerging stage. At this stage, NDVI, EVI, RDVI, OSAVI, RVI, DVI GEMI and expressly MSR increased dramatically. The IRG index is also another VI worthy to note. Also, the SR and EVI vegetation indices are higher during the flag leaf

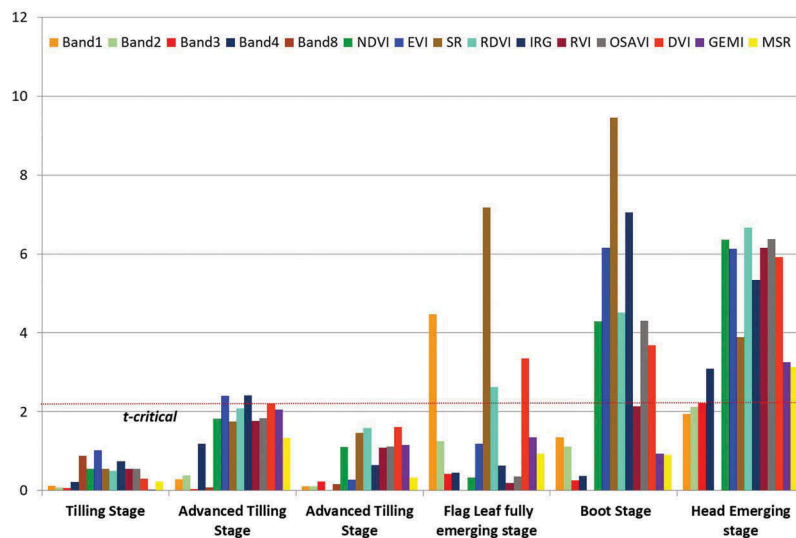


Figure 6. Graph of the t -test for area (a) (buried structure area) and area (b) (vegetated area) using bands (band1, band2, band3 and band4) and vegetation indices (NDVI, EVI, SR, RDVI, IRG, RVI, OSAVI, DVI, GEMI and MSR).

fully emerging stage and boot stage. One other valuable information extracted from this graph is that the IRG vegetation index is higher than other VIs during the tilling and advanced tilling stages as shown in Figure 6. Furthermore, as mentioned above, in the last two phenological stages (i.e. boot stage and head emerging stage) the absolute value of the test statistic is greater than the critical value (1.7), therefore we reject the null hypothesis and conclude that the research hypothesis is true. Comparing these results with results in Figure 5 it can be seen clearly that the boot stage and head emerging stage are most suitable for observing these vegetation anomalies over the buried structure.

Grid maps

The analysis of the spectral data (Figure 7) shows some of the main vegetation indices (NDVI, SR, GEMI, MSR) image maps for Area (a) and Area (b) during head emerging and flowering stages. In comparing Area (a) with Area (b) using NDVI index, Area (a) has lower values (average value 0.62) due to the existence of underground structures, while Area (b) has similar vegetation but higher NDVI index values (average value 0.77) due to the non-existence of structures. In addition, using MSR, Area (a) has higher values (average values 4.25) due to the existence of underground structures, while Area (b) has lower values (average values 1.85) due to the non-existence of structures. The red color illustrates high value of indices that distinguish the existence of structures. The existence of underground

structure can be clearly seen by comparing Area (a) with Area (b) for SR. Indeed, SR index obtains lower values (average value 7.24) in Area (a) than Area (b) with average value 12.58.

Using GEMI index, it can be seen that in target Area (a), the reflectance response (average value 950.69) is lower than in Area (b) (average value 1920.61), indicating that the resulting differences reinforce the inference of existence/non-existence of underground structures. It can be hypothesized that soil also contributed to the reflectance measurements. The variations between the two cases, namely, in the presence and in the absence of military underground structures, can result in better interpretations of images for the detection and identification of crops marks. This difference increases as the crop is growing.

Also, spectral indices are useful when applied to very high-resolution satellite images, aerial images or UAV images. Figure 7 shows the comparison using UAV image (was taken 27/3/2017) between field data image maps. It appears that the GEMI and MSR vegetation indices yield better results since the presence of the underground structure can more easily be identified. Figure 7 indicates a distinctive outcome using the SR, NDVI and GEMI vegetation indices.

The Vegetation Indices as determined by the in-situ measurements in Area (b) and Area (a) are shown in Figure 8. The average values of MSR and RVI indices in target Area (a) are higher than those in target Area (b); Even though, GEMI values are higher in Area (b) than Area (a). Similarly, NDVI,

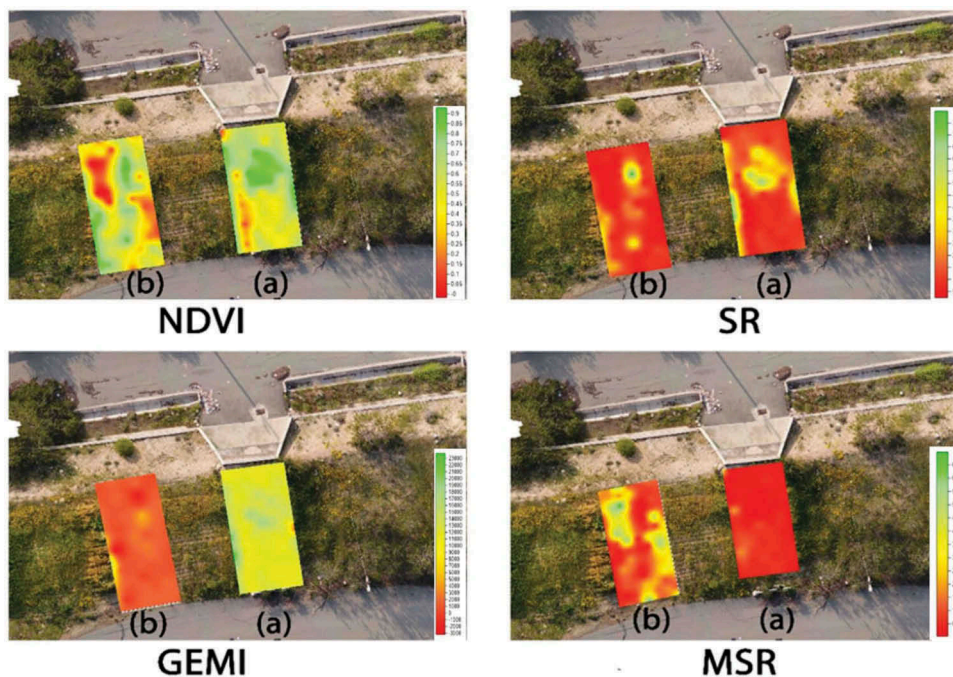


Figure 7. Comparison using UAV image between field data image maps for NDVI, SR, GEMI and MSR during head emerging and flowering stages.

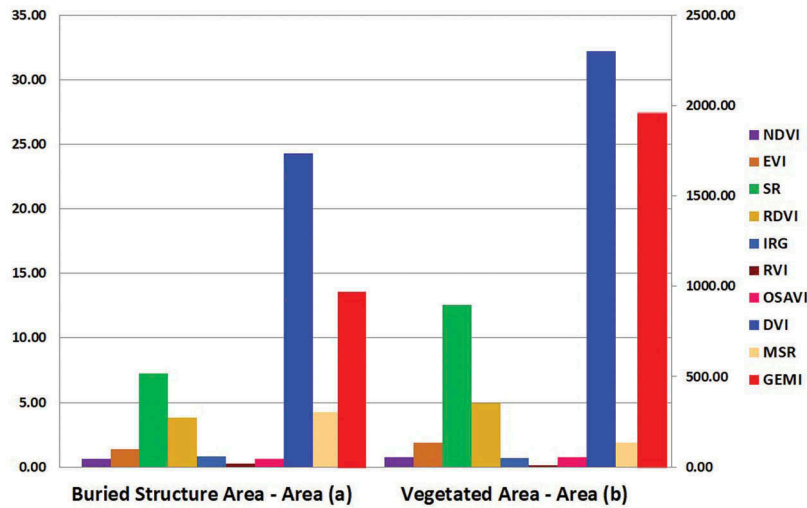


Figure 8. Comparison between the two study areas using the vegetation indices average values.

EVI, SR, RDVI, IRG, OSAVI and DVI are slightly higher in Area (b) than Area (a), the differences emphasize the existence/non-existence of underground structures.

Sentinel image processing

In situ spectroradiometric and UAV High resolution data are used to validate Sentinel -2A data at lower resolution acquired on 5/3/2017.

The modified Darkest Pixel (DP) method (Hadjimitsis, Clayton, & Hope, 2004a) was applied in the current study. The surface radiance of the dark targets is assumed to have approximated zero surface radiance or reflectance as shown by Hadjimitsis, Clayton, and Retalis (2004b) and Agapiou, Hadjimitsis, Papoutsas, Alexakis, and Papadavid (2011b). The modified Darkest Pixel (DP) atmospheric correction was applied for the

visible Bands of Sentinel data since it had been shown that DP is the most effective one for such spectral regions except the NIR (Agapiou et al., 2011b; Hadjimitsis & Clayton, 2008; Hadjimitsis et al., 2004b, 2004b). It is apparent that there is a fully compliance between the DP atmospheric corrected image reflectances (satellite data after atmospheric correction) with those acquired with the field spectroradiometer, as shown in Figure 9. DP does not work effectively in the NIR Bands due the water vapour absorption, as shown by Agapiou and Hadjimitsis (2011a) and this is shown revealed in this case; indeed, as seen in Figure 9, DP atmospheric corrected Sentinel reflectance values are lower than the field data. Meteorological data provided by the Department of Meteorology of Cyprus, were used in order to find whether any impact of the water vapour due to Relative Humidity have occurred during the satellite

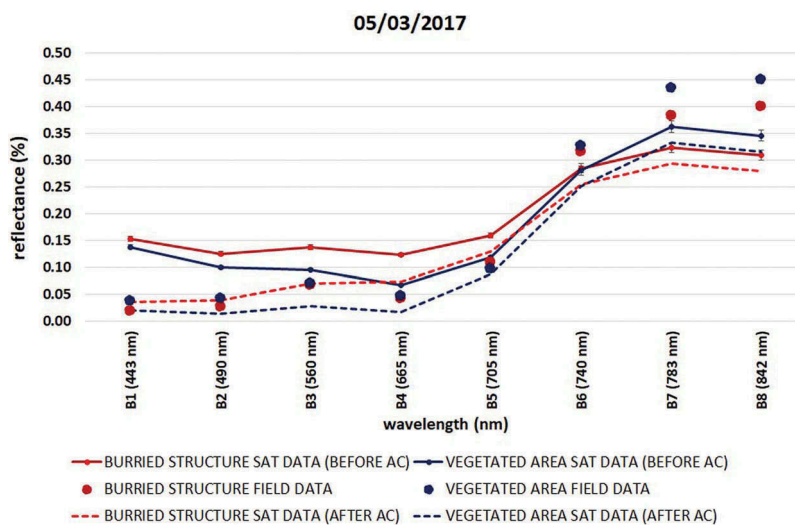


Figure 9. Comparison between the two study areas using satellite and field data before and after atmospheric correction on 5 March 2017.

overpass for the Sentinel NIR Bands. The relative humidity during the satellite overpass was 41%. As shown by Forster (1984) and Hadjimitsis et al. (2004a), relative humidity and temperature can be used to provide a measure of the equivalent mass of liquid water or water vapour thickness. Although the DP algorithm can be applied without any auxiliary meteorological data, as a fully image-based technique, the authors used these data to investigate any possible water vapour absorption effect in atmospheric correction as suggested by Agapiou et al. (2011b). The authors used Forster (1984) and McClatchey, Fenn, Selby, Volz, and Garing (1984) optical thickness values of water vapor calculation based on relative humidity and temperature. Indeed, the partial pressure of water vapour was calculated based on the ideal gas law assumption. Absorption, due to water vapor for wavelengths lower than $0.7 \mu\text{m}$, can be ignored as shown by Agapiou et al. (2011b) and Forster (1984).

Therefore, the assumption that absorption of water vapor for Sentinel blue green red Bands is zero, was made for the objective of this study. The optical thickness of water vapor, for the NIR of Sentinel was found to be $0.035 \mu\text{m}$. Based on the study by Agapiou et al. (2011b), it has been found that for water vapour values greater than $0.026 \mu\text{m}$ the water vapour absorption was significant and with a “non-additive” effect. Indeed, in this case, the absorption affects the satellite signal in the NIR (Band 5 to Band 8) as shown in Figure 9 but not with an additive effect as the one occurred with the visible Sentinel Bands in which scattering is the main atmospheric effect. This was also confirmed by using the Pseudo Invariant Targets (PIT’s) atmospheric correction method (Themistocleous, Hadjimitsis,

Retalis, & Chrysoulakis, 2012), in which the intercept of the linear regression by using standard non-variant targets in the vicinity of this area shows a similar absorption effect in the NIR sentinel Bands. Correspondingly, the resulting reflectance spectrum in Figure 9 before atmospheric correction of Vegetated area data throughout Band 6 to Band 8 was always at a higher level than the Buried structure data. It can clearly be seen using Satellite and Field data. In addition, it is evident that Buried structure Satellite data is lower than Vegetated area satellite data after atmospheric correction. This verifies that ground spectroradiometric data and Satellite data are in close proximity and therefore have similar results: the Vegetated area has higher reflectance values than the Buried structure area, indicating the effect of the presence/non – presence of underground structure.

In addition, Figure 10 shows the comparison between the two study areas using Satellite (after atmospheric correction) and Field data regarding Vegetation Indices. It is obvious that the results are similar. Specifically, Vegetated Area using Satellite Data comparing with its field Data their values are almost identical. Furthermore, Vegetated Areas results are higher than Buried Structure Satellite and Field data, especially using SR and NDVI vegetation indices. Additionally, Buried Structure and Vegetated field data are very close with the respective Satellite Data. Overall there are differences between the two areas using Field Data as well as in Satellite Data due the existence and non-existence of underground buried structure.

Concluding remarks

Field spectroscopy can support Satellite Remote Sensing studies for systematically monitoring critical

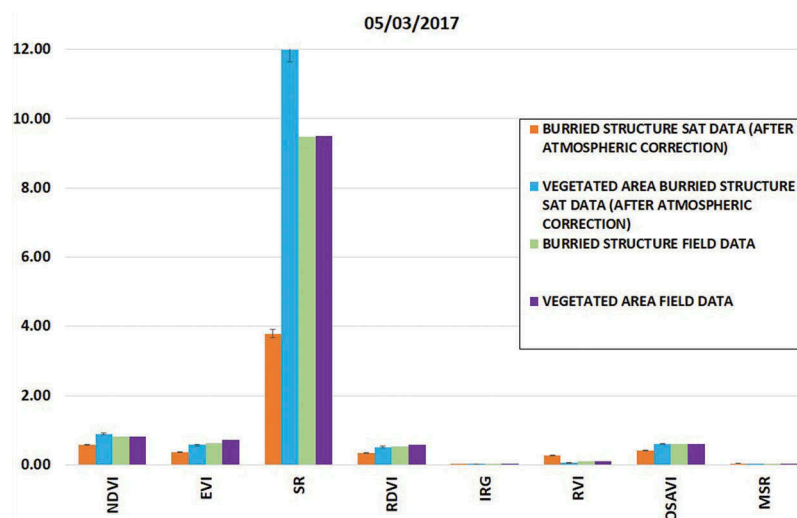


Figure 10. Vegetation indices comparison between the two study areas using satellite and field data after atmospheric correction on 5 March 2017.

areas of interest including detection of underground bunkers.

The application of remote sensing in defense and security merges the technological improvements of remote sensing sensors with military needs to improve the quality of information retrieved from remote sensing data.

The advantages of using vegetation indices as proxy variables for inter-calibration among existing sensors are the low sensitivity to the uncertainties in atmospheric correction and the variation in the satellite viewing angle (Steven et al., 2003). As shown in this paper, vegetation indices can corroborate areas of possible military underground structures.

In comparing the two areas, the findings (Figure 7–10) reveal differences between them. This is clear in Figure 7, where image maps illustrate the differences between the two areas. NDVI, SR and MSR, mostly GEMI vegetation index is useful for determining areas where military underground structures are present. Spectroradiometric measurements can be used as an alternative approach to identify underground military structures, since they can provide accurate spectral signatures for a wide spectral region. Anomalies of the crop spectral signatures resulting from an existing underground structure can be recorded using a spectroradiometer.

Using the NIR Band of Sentinel-2A could be useful to identify the underground structure. It is apparent that the wave Band analysis performed on Sentinel 2 data distinguishes between the two study sites. Monitoring variations of the NIR spectrum during the life cycle of vegetation is a key parameter in Field spectroscopy for the detection of military underground structures using remote sensing techniques.

In this study, it was demonstrated how remote sensing can be exploited as a monitoring and decision-making tool by any agency in tackling military and security issues related to the presence of underground military structures. Field spectroscopy measurements were used to detect underground military structures through variations in vegetation indices. Indeed, vegetation indices can be used to develop a suitable vegetation index for detecting military underground structures. Additionally, remote sensing images may be used for Field spectroscopy for the detection of those structures.

Areas covered by natural soil where underground structures are present or absent can easily be detected as a result of the change in the spectral signature of the overlying vegetation; in this respect, vegetation indices, such as the NDVI, SR, RVI, OSAVI, DVI, GEMI and MSR, may be used for this purpose.

Further testing and field spectroradiometric measurements will be performed to study other types of military underground structures to evaluate the above results and the satellites' spectral sensitivity. The development of a standard model/methodology

framework to be produced through the stages of the study for locating military underground structures is an innovation in military operations research. Additionally, an unmanned aerial vehicle (UAV) may be used to survey the area with visible and near-infrared cameras to generate other Vegetation Indices for comparison to the in-situ spectroradiometric measurements (Melillos et al., 2016b). The methodology presented in this study can be further extended to other satellite sensors, especially to those on board the next new generation high-resolution satellites.

Acknowledgments

The authors would like to also acknowledge Sentinel-2 imagery from European Space Agency (ESA)

Disclosure statement

No potential conflict of interest was reported by the authors.

References

- Agapiou, A., & Hadjimitsis, D. (2011a). Vegetation indices and field spectroradiometric measurements for validation of buried architectural remains: Verification under area surveyed with geophysical campaigns. *Journal of Applied Remote Sensing*, 5(1), 53554.
- Agapiou, A., Hadjimitsis, D.G., & Alexakis, D.D. (2012b). Evaluation of broadBand and narrowBand vegetation indices for the identification of archaeological crop marks. *Remote Sensing*, 4(12), 3892–3919.
- Agapiou, A., Hadjimitsis, D.G., Alexakis, D.D., & Papadavid, G. (2012a). Examining the phenological cycle of barley (*Hordeum Vulgare*) using satellite and in situ spectroradiometer measurements for the detection of buried archaeological remains. *GIScience & Remote Sensing*, 49(6), 854–872.
- Agapiou, A., Hadjimitsis, D.G., Papoutsas, C., Alexakis, D. D., & Papadavid, G. (2011b). The importance of accounting for atmospheric effects in the application of NDVI and interpretation of satellite imagery supporting archaeological research: The case studies of Palaepaphos and Nea Paphos sites in Cyprus. *Remote Sensing*, 3(12), 2605–2629.
- Agapiou, A., Hadjimitsis, D.G., Sarris, A., Georgopoulos, A., & Alexakis, D.D. (2013). Optimum temporal and spectral window for monitoring crop marks over archaeological remains in the Mediterranean region. *Journal of Archaeological Science*, 40(3), 1479–1492.
- Apparao, A., Gangadhara Rao, T., Sivarama Sastry, R., & Subrahmanya Sarma, V. (1992). Depth of detection of buried conductive targets with different electrode arrays in resistivity prospecting. *Geophysical Prospecting*, 40(7), 749–760.
- ARO. (2018). Detection of underground installations in hostile environments. Retrieved from <http://www.cs.tau.ac.il/~nin/papers/ARORep9Feb10.pdf>

- Canada Centre for Remote Sensing. (2016). Tutorial: Fundamentals of remote sensing. Retrieved from <http://www.nrcan.gc.ca/node/9309>
- Chen, J.M. (1996). Evaluation of vegetation indices and a modified simple ratio for boreal application. *Canadian Journal of Remote Sensing*, 22, 229–242.
- Crothers, B.M., Lanphear, J.M., Garino, M.B., Konyha, M. P.P., III, & Byrne, E.M.P. (1967). US space-based intelligence, surveillance, and reconnaissance ISR and space systems. Retrieved from <https://pdfs.semanticscholar.org/8ea3/f79e3814511195949a3923c35f9bd7ab38c1.pdf>
- D'Oleire-Oltmanns, S., Marzolf, I., Peter, K.D., & Ries, J.B. (2012). Unmanned aerial vehicle (UAV) for monitoring soil erosion in Morocco. *Remote Sensing*, 4(11), 3390–3416.
- Headquarters, Department of the Army. (2006). *Human intelligence collector operations field manual no. 2–22.3 (FM 34–52)*. Washington.
- Domínguez Galindo, R.E., Bandy, W.L., Mortera Gutiérrez, C.A., & Ortega Ramírez, J. (2013). Geophysical-archaeological survey in lake Tequesquitengo, Morelos, Mexico. *Geofísica Internacional*, 52(3), 261–275.
- ESA. (2018). Sentinel-2A satellite sensor, satellite imaging corp. Retrieved from <https://www.satimagingcorp.com/satellite-sensors/other-satellite-sensors/sentinel-2a/>
- Forster, C.B. (1984). Derivation of atmospheric correction procedures for LANDSAT MSS with particular reference to urban data. *International Journal of Remote Sensing*, 5 (5), 799–817.
- Gamon, J.A., & Surfus, J.S. (1999). Assessing leaf pigment content and activity with a reflectometer. *New Phytologist*, 143, 105–117.
- Garaba, S.P., & Zielinski, O. (2015). An assessment of water quality monitoring tools in an estuarine system. *Remote Sensing Applications: Society and Environment*, 2, 1–10.
- Giardino, M.J.A. (2011). History of NASA remote sensing contributions to archaeology. *Journal of Archaeological Science*, 38(9), 2003–2009.
- Gunn, D.A., Marsh, S.H., Gibson, A., Ager, G.J., McManus, K.B., Caunt, S., & Culshaw, M.G. (2008). Remote thermal IR surveying to detect abandoned mine-shafts in former mining areas. *Quarterly Journal of Engineering Geology and Hydrogeology*, 41(3), 357–370.
- Hadjimitsis, D.G., & Clayton, C.R.I. (2008). The use of an improved atmospheric correction algorithm for removing atmospheric effects from remotely sensed images using an atmosphere-surface simulation and meteorological data. *Meteorological Applications*, 15(3), 381–387.
- Hadjimitsis, D.G., Clayton, C.R.I., & Hope, V.S. (2004a). An assessment of the effectiveness of atmospheric correction algorithms through the remote sensing of some reservoirs. *International Journal of Remote Sensing*, 25(18), 3651–3674.
- Hadjimitsis, D.G., Clayton, C.R.I., & Retalis, A. (2004b). On the darkest pixel atmospheric correction algorithm: A revised procedure applied over satellite remotely sensed images intended for environmental applications. *SPIE Proceedings*, 5239, 464–471.
- Huete, A.R., Liu, H.Q., Batchily, K., & van Leeuwen, W. (1997). A comparison of vegetation indices over a global set of TM images for EOS-MODIS. *Remote Sensing of Environment*, 59(3), 440–451.
- International Ocean-Colour Coordinating Group (IOCCG). (2008). *Why ocean colour? The societal benefits of ocean-colour technology*. Report No. 7. T. Platt, N. Hoepffner, V. Stuart, & C. Brown (Eds.). (pp. 147). Dartmouth, Canada: IOCCG
- IOSS (2017). Interagency OPSEC support staff [OPSEC glossary of terms]. Retrieved from http://www.au.af.mil/au/awc/awcgate/documents/opsec_definitions.htm
- Johnson, J.K. (2006). *Remote sensing in archaeology: An explicitly north American perspective*. The University of Alabama Press, Tuscaloosa, Alabama.
- Jordan, C.F. (1969). Derivation of leaf area index from quality of light on the forest floor. *Ecology*, 50, 663–666.
- Kelly, R.E. (2001). Underground structure detection by surface magnetic gradient measurements. *SPIE Proceedings*, 4491, 367–374.
- KMC. (2008). Priddy Mines: A walk through history.
- Lasaponara, R., & Masini, N. (2006). Identification of archaeological buried remains based on the normalized difference vegetation index (NDVI) from quickbird satellite data. *IEEE Geoscience and Remote Sensing Letters*, 3(3), 325–328.
- Lasaponara, R., & Masini, N. (2007). Detection of archaeological crop marks by using satellite quickbird multi-spectral imagery. *Journal Archaeological Science*, 34(2), 214–221.
- Mahrer, K.D. (1995). Radio frequency electromagnetic tunnel detection and delineation at the Otay Mesa site. *Geophysics*, 60(2), 413.
- McClatchey, R.A., Fenn, W.S., Selby, J.E.A., Volz, F.E., & Garing, J.S. (1984). *Optical properties of the atmosphere* (3rd ed.). Bedford, MA, USA: Rep. AFCrl-71-0279, 85, Air Force Cambridge Res. Lab. Retrieved from <https://apps.dtic.mil/docs/citations/AD0753075>
- Melillos, G., Themistocleous, K., Papadavid, G., Agapiou, A., Michaelides, S., Prodromou, M., & Hadjimitsis, D.G. (2016a). Integrated use of field spectroscopy and satellite remote sensing for defence and security applications in Cyprus. *SPIE Proceedings*, 9823. doi:10.1117/12.2241207
- Melillos, G., Themistocleous, K., Papadavid, G., Agapiou, A., Prodromou, M., Michaelides, S., & Hadjimitsis, D.G. (2016b). Importance of using field spectroscopy to support the satellite remote sensing for underground structures intended for security reasons in the eastern Mediterranean region. *SPIE Proceedings*, 9988. doi:10.1117/12.2240714
- Milton, E.J., & Rollin, E.M. (2006). Estimating the irradiance spectrum from measurements in a limited number of spectral bands. *Remote Sensing of Environment*, 100 (3), 348–355.
- Novo, A., Solla, M., Fenollós, J.L.M., & Lorenzo, H. (2014). Searching for the remains of an early bronze age city at Tell Qubr Abu Al-'Atiq (Syria) through archaeological investigations and GPR imaging. *Journal of Cultural Heritage*, 15(5), 575–579.
- Papadavid, G., Hadjimitsis, D., Michaelides, S., & Nisantzi, A. (2011). Crop evapotranspiration estimation using remote sensing and the existing network of meteorological stations in Cyprus. *Advances in Geosciences*, 30, 39–44.
- Pearson, R.L., & Miller, L.D. (1972, October 2–6). Remote mapping of standing crop biomass and estimation of the productivity of the short grass prairie. *Proceedings of the 8th international symposium on remote sensing of environment* (pp. 1357–1381). Ann Arbor, Michigan USA: Willow Run Laboratories, Environmental Research Institute of Michigan
- Pinty, B., & Verstraete, M.M. (1992). GEMI: A non-linear index to monitor global vegetation from satellites. *Vegetatio*, 101(1), 15–20.

- Piper, J.E., Lim, R., Thorsos, E.I., & Williams, K.L. (2009). Buried sphere detection using a synthetic aperture sonar. *IEEE Journal of Oceanic Engineering*, 34(4), 485–494.
- Richelson, J.T. (2013). *Underground Facilities: Intelligence and Targeting Issues*. The National Security Archive. Electronic Briefing book, No. 439, Washington D.C.. Retrieved from <https://nsarchive2.gwu.edu/NSAEBB/NSAEBB439/>
- Riley, D.N. (1979). Factors in the development of crop marks. *Aerial Archaeology*, 4, 28–32.
- Rondeaux, G., Steven, M., & Baret, F. (1996). Optimization of soil-adjusted vegetation indices. *Remote Sensing of Environment*, 55, 95–107.
- Roujean, J.-L., & Breon, F.-M. (1995). Estimating PAR absorbed by vegetation from bidirectional reflectance measurements. *Remote Sensing of Environment*, 51, 375–384.
- Rouse, J.W., Jr., Haas, R.H., Schell, J.A., Deering, D.W., & Harlan, J.C. (1974). *Monitoring the vernal advancements and retrogradation (greenwave effect) of nature vegetation. Type II I report for the period September 1972–November 1974*. USA: Remote Sensing Center Texas A&M University College Station, Texas 77843. Retrieved from <https://ntrs.nasa.gov/archive/nasa/casi.ntrs.nasa.gov/19750020419.pdf>
- Sarris, A., Galaty, M.L., Yerkes, R.W., Parkinson, W.A., Gyucha, A., Billingsley, D.M., & Tate, R. (2004). Geophysical prospection and soil chemistry at the early copper age settlement of Vésztó-Bikeri, southeastern Hungary. *Journal of Archaeological Science*, 31(7), 927–939.
- Sarris, A., Papadopoulos, N., Agapiou, A., Salvi, M.C., Hadjimitsis, D.G., Parkinson, W.A., ... Duffy, P.R. (2013). Integration of geophysical surveys, ground hyperspectral measurements, aerial and satellite imagery for archaeological prospection of prehistoric sites: The case study of Vésztó-Mágor Tell, Hungary. *Journal of Archaeological Science*, 40(3), 1454–1470.
- Sepp, E.M. (2000). *Deeply buried facilities: Implications for military operations*. Occasional paper No. 14. Center for Strategy and Technology. Alabama, USA: Air War College Air University Maxwell Air Force Base. Retrieved from <https://apps.dtic.mil/dtic/tr/fulltext/u2/a425461.pdf>
- Steven, M.D., Malthus, T.J., Baret, F., Xu, H., & Chopping, M.J. (2003). Intercalibration of vegetation indices from different sensor systems. *Remote Sensing of Environment*, 88(4), 412–422.
- Stolarczyk, L.G. (1993, April 26–29). Gradiometer antennas for detection of tunnels by scattered electromagnetic waves. *Proceedings of the 4th Tunnel Detection Symposium on Subsurface Exploration Technology*. Golden, Colorado, USA. Retrieved from <https://apps.dtic.mil/dtic/tr/fulltext/u2/a276372.pdf>
- Themistocleous, K., Agapiou, A., Cuca, B., & Hadjimitsis, D.G. (2015). Unmanned aerial systems and spectroscopy for remote sensing applications in archaeology. *International Archives of the Photogrammetry, Remote Sensing and Spatial Information Sciences - ISPRS Archives*, 40, 1419–1423.
- Themistocleous, K., Hadjimitsis, D.G., Retalis, A., & Chrysoulakis, N. (2012). Development of a new image based atmospheric correction algorithm for aerosol optical thickness retrieval using the darkest pixel method. *Journal of Applied Remote Sensing*, 6(1), 063538.
- Tucker, C.J. (1979). Red and photographic infrared linear combinations for monitoring vegetation. *Remote Sensing of Environment*, 8, 127–150.
- Winton, H., & Horne, P. (2010). National archives for national survey programmes: NMP and the English heritage aerial photograph collection. In D. Cowley, R. A. Standring, & M.J. Abicht (Eds.), *Landscapes through the lens: Aerial photographs and historic environment* (pp. 7–18). Oxford: Oxbow Books.
- Zhang, Y., Liao, X., & Carin, L. (2004). Detection of buried targets via active selection of labeled data: Application to sensing subsurface UXO. *IEEE Transactions on Geoscience and Remote Sensing*, 42(11), 2535–2543.